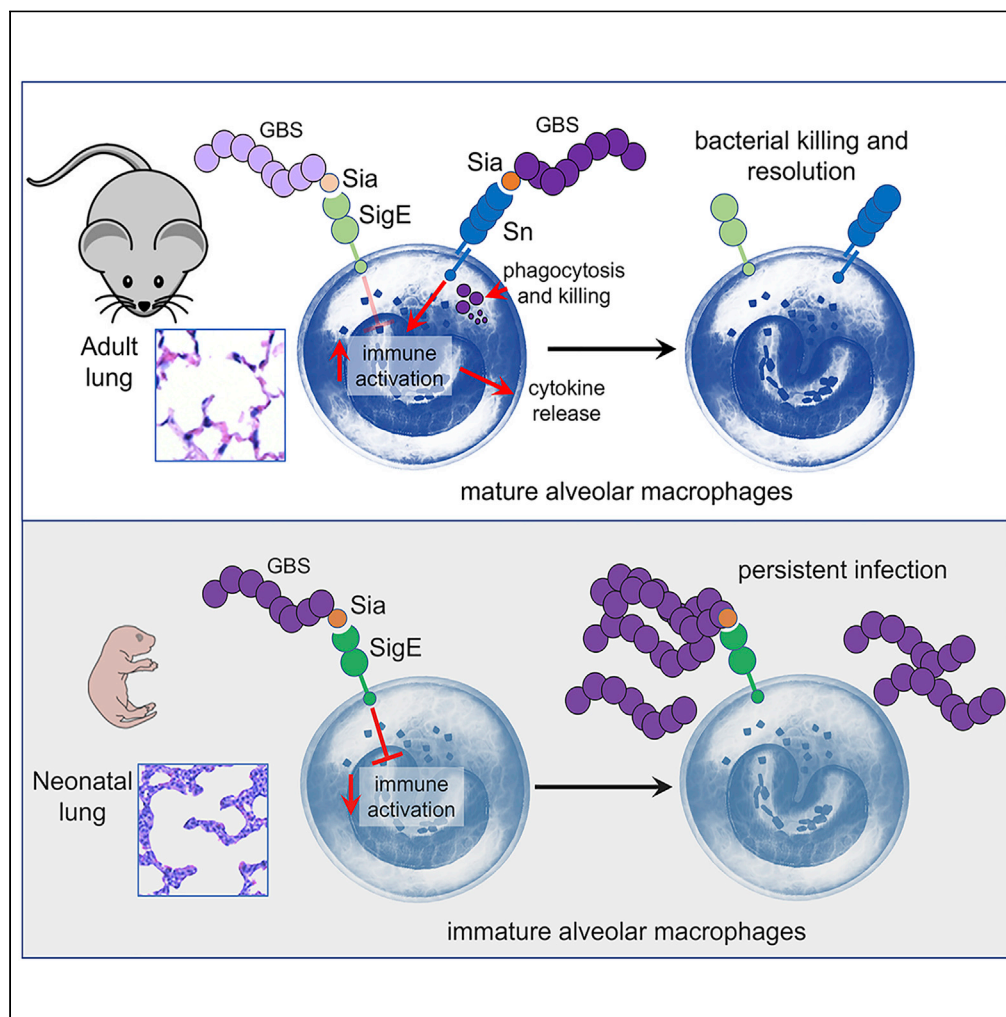**Article**

Developmental Immaturity of Siglec Receptor Expression on Neonatal Alveolar Macrophages Predisposes to Severe Group B Streptococcal Infection

Sean J. Lund,
Kathryn A. Patras,
Jacqueline M.
Kimmey, ..., Omar
Lakhdari, Victor
Nizet, Lawrence S.
Prince

lprinceucsd@gmail.com

HIGHLIGHTS

Newborn mice fail to kill GBS, developing persistent lung injury

Mature AMΦ detect the Sialic acid capsule on GBS to mediate bacterial clearance

Immature newborn AMΦ lack mature Siglec expression required for killing GBS

GBS engages the inhibitory Siglec-E on newborn AMΦ to suppress innate immunity

iScience

Article

Developmental Immaturity of Siglec Receptor Expression on Neonatal Alveolar Macrophages Predisposes to Severe Group B Streptococcal Infection

Sean J. Lund,[1] Kathryn A. Patras,[1] Jacqueline M. Kimmey,[1,2] Asami Yamamura,[1] Lindsay D. Butcher,[1] Pamela G.B. Del Rosario,[1] Gilberto E. Hernandez,[1] Alyssa M. McCoy,[1] Omar Lakhdari,[1] Victor Nizet,[1] and Lawrence S. Prince[1,3,*]

SUMMARY

***Streptococcus agalactiae* (Group B *Streptococcus*, GBS) is the most common neonatal pathogen. However, the cellular and molecular mechanisms for neonatal susceptibility to GBS pneumonia and sepsis are incompletely understood. Here we optimized a mouse model of GBS pneumonia to test the role of alveolar macrophage (AMΦ) maturation in host vulnerability to disease. Compared with juvenile and adult mice, neonatal mice infected with GBS had increased mortality and persistence of lung injury. In addition, neonatal mice were defective in GBS phagocytosis and killing. AMΦ depletion and disruption of AMΦ differentiation in *Csf2*−/− mice both impaired GBS clearance. AMΦ engage the heavily sialylated GBS capsule via the cell surface Siglec receptors Sn and Siglec-E. Although both newborn and adult AMΦ expressed Siglec-E, newborn AMΦ expressed significantly lower levels of Sn. We propose that a developmental delay in Sn expression on AMΦ may prevent effective killing and clearing of GBS from the newborn lung.**

INTRODUCTION

The encapsulated gram-positive bacterium *Streptococcus agalactiae* (group B *Streptococcus*, GBS) remains a potentially devastating neonatal pathogen. Globally, GBS colonizes the vaginal or rectal epithelium of an estimated 21.7 million pregnant women (Russell et al., 2017). The leading infectious cause of neonatal mortality, GBS, is estimated to cause 150,000 newborn deaths worldwide each year (Madrid et al., 2017; Seale et al., 2017). Infants are exposed to GBS during passage through the birth canal or via ascending infection through the amniotic membranes. GBS neonatal disease is commonly classified as early-onset (<7 days of age) or late-onset disease (7 days–6 months of age) (Baker and Barrett, 1973; Franciosi et al., 1973; Horn et al., 1974; Randis et al., 2017). In the majority of cases of early-onset disease, newborns aspirate contaminated amniotic or vaginal fluid, developing clinical signs of pneumonia, lung injury, and sepsis within the first few hours of life. In contrast, late-onset GBS infections tend to present days later with bacteremia and a high risk of meningitis (Raabe and Shane, 2019). Serious GBS infections in otherwise healthy older children and adults are rare, although non-pulmonary invasive disease is increasingly reported in individuals with lowered immunity such as the elderly, pregnant women, and those with diabetes or cancer (Pitts et al., 2018; Skoff et al., 2009).

In this study, we sought a mechanistic understanding of the unique susceptibility of the newborn infant to severe invasive GBS infection initiated through the lung portal of entry. Normally, multiple cell populations serve to protect the lung from infection and injury. Epithelial cells secrete surfactant and antimicrobial peptides capable of killing and/or inactivating inhaled microbes (Weitnauer et al., 2016; Whitsett and Alenghat, 2015). In addition, mucociliary clearance captures and removes particulates and infectious agents (Fliegauf et al., 2013). The major resident immune cells protecting the lung from inhaled pathogens are alveolar macrophages (AMΦs). Present throughout life, AMΦs can phagocytose and kill microbes, release inflammatory mediators, recruit additional immune cells including neutrophils, and participate in tissue repair following injury (Allard et al., 2018; Byrne et al., 2015; Kopf et al., 2015). AMΦ differentiation in the postnatal lung is

driven by epithelial GM-CSF production and cell-autonomous TGF-β signaling (Berclaz et al., 2002; Schneider et al., 2014; Shibata et al., 2001; Yu et al., 2017). Newborn AMΦ may therefore lack the fully differentiated phenotype present in older children and adults (Guilliams et al., 2013). The unique susceptibility of the neonate to severe GBS pneumonia and sepsis could implicate AMΦ immaturity and/or a deficiency in other components of lung immunity.

Identifying the cellular and molecular mechanisms of newborn GBS pneumonia requires development and optimization of a translatable experimental model. Here we provide data from a neonatal mouse model that recapitulates many key aspects of human GBS disease, including the timing of mortality from lung disease and later-onset bacteremia and CNS involvement. We find that the inability of neonatal mice to kill GBS and resolve lung injury correlates to AMΦ immaturity at birth, and in particular a differential kinetic expression of two key lectin receptors (Siglecs) that bind the sialic acid-containing GBS exopolysaccharide capsule (CPS), an essential virulence determinant of the pathogen. Identifying a cellular basis of neonatal GBS susceptibility highlights principles of developmental immunity and pathogen molecular mimicry potentially amenable to therapeutic targeting, with an eye to augmenting neonatal AMΦ development and closing a high-risk window for lethal GBS infections.

RESULTS

Increased Mortality and Persistence of Lung Injury in Neonatal GBS Infection

Despite being the most common cause of neonatal pneumonia, the molecular and cellular mechanisms responsible for the unique susceptibility of newborns to GBS remain unclear. To investigate key host-pathogen interactions in the newborn period, we developed and employed a murine model of GBS neonatal pneumonia (see Transparent Methods). Newborn C57BL/6 mice were lightly anesthetized and intranasally inoculated with 28,000 CFU/g of wild-type (WT) GBS (serotype III strain COH1). Control mice were similarly anesthetized and received an identical volume of sterile, endotoxin-free saline. For comparison, we also infected juvenile (PND7) and adult (8-week-old) mice with a comparable weight-based GBS inoculum. Adult and juvenile mice universally survived infection (Figure 1A). However, in neonatal mice, over 20% of GBS-infected animals died within 2 days. We did not observe additional deaths in any group between days 2 and 7.

We cultured GBS from infected lungs to compare bacterial clearance between neonatal, juvenile, and adult mice (Figure 1B). Adult mice did have viable GBS bacterial CFUs in their lungs 1 day after infection but no GBS when measured at day 3. Two adult mice did have rare detectable GBS on day 7 after infection. Juvenile and neonatal mouse lungs contained viable GBS when measured both 1 and 3 days after infection. We next measured temporal changes in lung pathology following GBS infection. All ages of mice infected with GBS developed histological signs of significant acute lung injury 1 day following infection (Figures 1C and 1D). However, adult mice infected with GBS showed rapid histological improvement by day 3 and complete resolution by day 7. By comparison, abnormal pathology in GBS-infected juvenile mice persisted to day 3 with resolution by day 7. Pathology in GBS-infected neonatal mice was even more persistent, with no improvement as late as 7 days post infection. Our GBS infection model therefore replicates the clinical scenario of early-onset GBS disease, which includes severe pneumonia, lung injury, and death specifically in neonates. In addition, these initial experiments suggest neonates have defects related to clearance of GBS and resolution of lung injury.

Delayed Kinetics of Lung Inflammation and GBS Clearance by Alveolar Macrophages in Neonatal GBS Pneumonia

The very distinct differences in GBS clearance and resolution of lung pathology between newborn and adult mice suggested potential differences in the lung immune response and inflammatory signaling. To initially test the innate immune response to GBS, we measured expression of pro-inflammatory mediators *Il1b*, *Il6*, and *Cxcl1* in the first 24 h following GBS infection. Adult mice had elevated levels of each inflammatory mediator during the 2- to 12-h time window following GBS infection; however, expression levels of the factors fell back to baseline by 24 h (Figure 2A). By contrast in neonatal mice, expression of *Il1b*, *Il6*, and *Cxcl1* did not increase until 24 h after GBS infection (Figure 2B), revealing a delayed inflammatory response in neonatal mouse lungs compared with adults. Adult lungs had a rapid influx of additional CD68+ macrophages and monocytes into the lung 12–24 h after GBS inoculation; however, neonatal lungs did not show such an accumulation of CD68+ cells 24 h after infection (Figure 2C). This finding corresponded to the delay in the upregulation of key inflammatory mediators and chemoattractants. Thus the neonatal lung immune
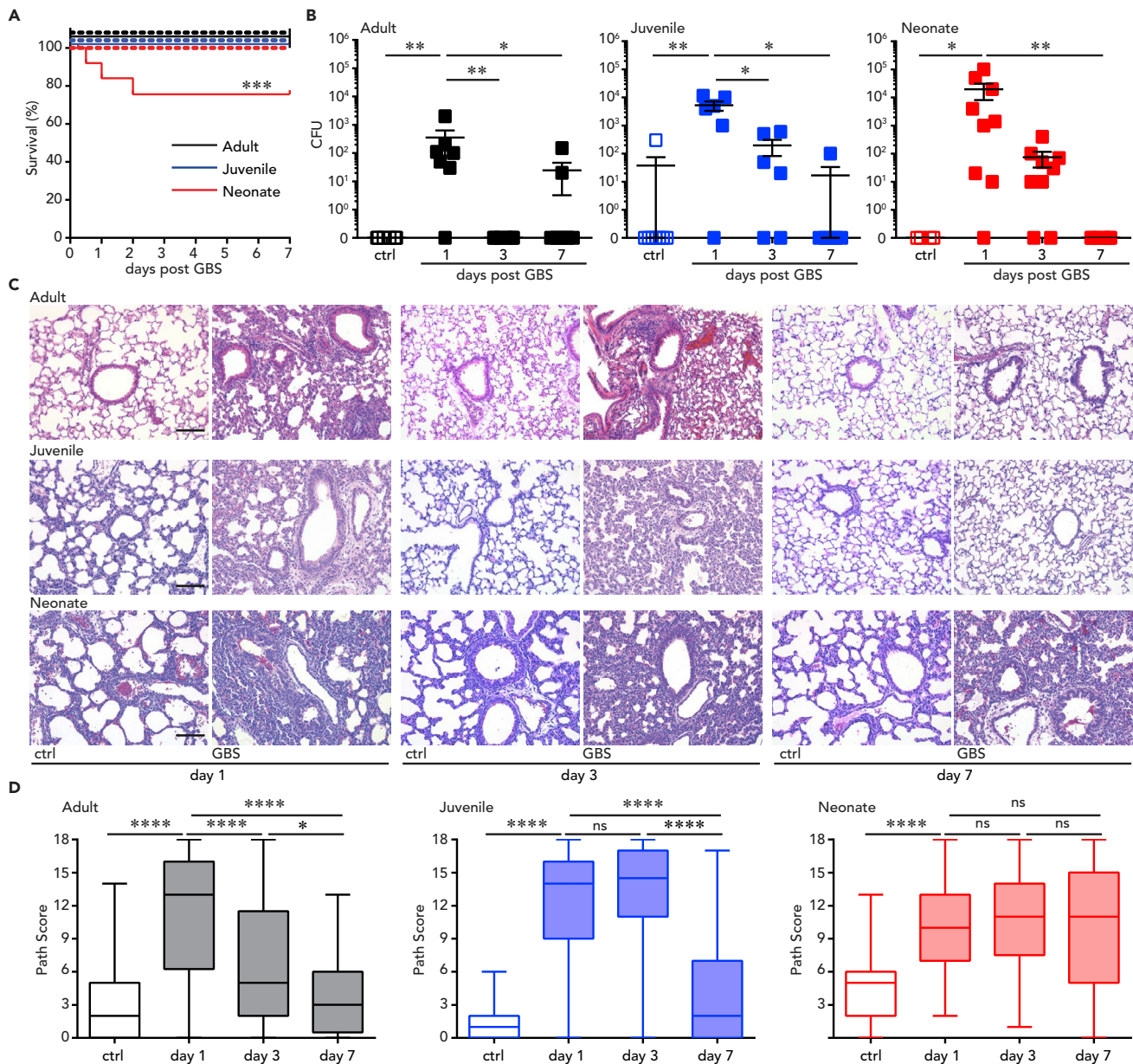
Figure 1. Increased Mortality and Persistence of Lung Injury in Neonatal GBS Infection

(A) Kaplan-Meier survival curve showing increased mortality in neonatal mice infected with intranasal GBS. All mice were given 28,000 CFU/g body weight of GBS. Neonatal mice (red) were infected within 24 h of delivery, juvenile mice (blue) were infected on day 7 of life, adult mice (black) were 6–8 weeks of age at infection. GBS-infected animals are shown with solid lines. Controls (dashed lines) were given identical anesthesia but intranasal sterile saline. ***$p < 0.005$ using the Mantel-Cox test (n = 15–29).

(B) CFU recovered from lung 1, 3, and 7 days after infection from adults, juvenile, and neonatal mice. Data are represented as mean $\pm$ SEM. *$p < 0.05$, **$p < 0.01$ using Mann-Whitney U test (n = 6–9).

(C) Representative H&E-stained sections obtained from mouse lungs 1, 3, and 7 days after GBS infection demonstrates initial lung injury and inflammation in all mice, with differential resolution by day 7. Scale bar, 100 μm.

(D) Neonatal mice displayed persistence of lung pathology following GBS infection. Lung pathology scoring was performed by three independent, blinded reviewers. Each experimental group included four to six animals with three representative images taken in a systematic method from each animal for a total of 12–18 images per group. The box is bound by the 25th and 75th percentile; the middle line represents the median value. The whiskers represent the minimum and maximum values. *$p < 0.05$, **$p < 0.01$, ***$p < 0.005$, ****$p < 0.001$ using one-way ANOVA.
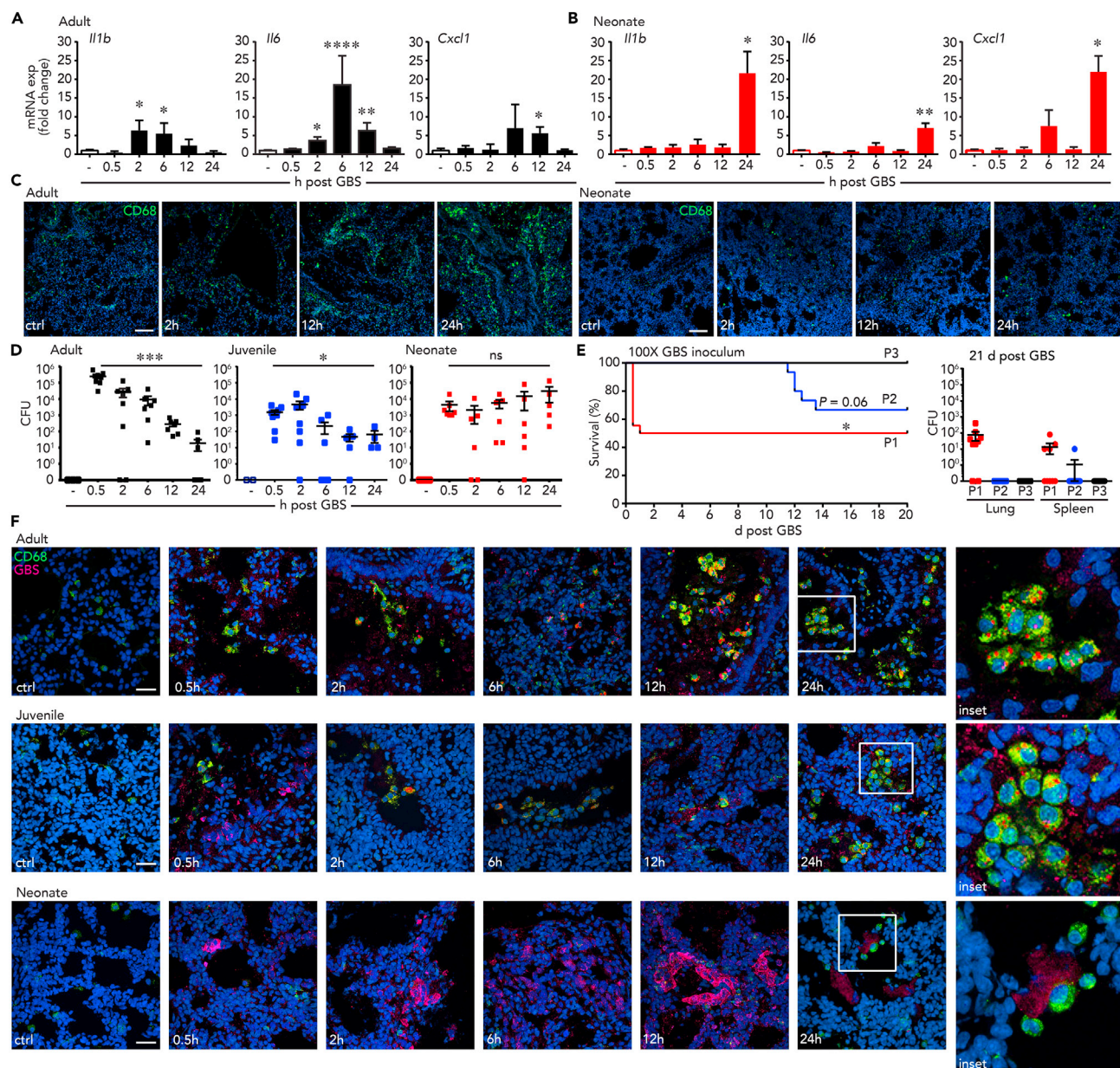
Figure 2. Delayed Kinetics of Lung Inflammation and GBS Clearance by Alveolar Macrophages in Neonatal GBS Pneumonia

(A) In adult mice, GBS infection induced inflammatory mediator expression in lung tissue between 2 and 6 h post infection. mRNA expression measured by real-time PCR and represented as fold change compared with control animals using *Gapdh* for normalization. Levels of *Il1b*, *Il6*, and *Cxcl1* all fell to baseline values by 24 h. Data are represented as mean $\pm$ SEM. Significance calculated using ΔC_T values. *$p < 0.05$, **$p < 0.01$, ****$p < 0.001$ using unpaired t test. (n = 5–8 mice per time point).

(B) In contrast to adult mice, increased expression of *Il1b*, *Il6*, and *Cxcl1* in neonatal mice was not detected until 24 h after GBS infection. Significance calculated using ΔC_T values. *$p < 0.05$, **$p < 0.01$ using unpaired t test. (n = 4–6 mice per time point).

(C) Differential accumulation of CD68^{+} inflammatory cells in the lungs of adult mice following GBS infection compared with neonates. Confocal immunofluorescence micrographs showed accumulation of CD68^{+} cells (green) within 12–24 h after GBS infection in adults. Neonatal lungs did not display similar cellular accumulation. Images representative of two to three separate experiments. Cell nuclei stained with DRAQ5 (blue). Scale bar, 100 μm.

(D) Lack of GBS clearance in neonatal mouse lungs. GBS CFU recovered from the lungs of adult, juvenile, and neonatal mice were measured 0.5, 2, 6, 12, and 24 h after infection. Data are represented as mean $\pm$ SEM. *$p < 0.05$, **$p < 0.01$, ***$p < 0.005$ using Mann-Whitney U test (n = 6–9).

(E) Susceptibility to GBS infection was unique to newborn mice. Left panel shows Kaplan-Meier survival curve from neonatal mice infected with GBS (2.8×10^6 CFU/g body weight) on postnatal day 1 (red), postnatal day 2 (blue), and postnatal day 3 (black). *$p < 0.05$ using the Mantel-Cox test (n = 10–17). Right panel shows GBS CFU recovered from lung and spleen from surviving animals 21 days after infection. Systemic persistence of infection was primarily detected in mice infected on P1. Data are represented as mean $\pm$ SEM.

Figure 2. *Continued*

(F) Uptake of GBS by CD68^{+} lung macrophages. Confocal immunofluorescent micrographs show localization of GBS (red) within CD68^{+} cells (green) soon after infection in adult and juvenile mouse lungs. However, in neonatal lungs, GBS uptake by CD68^{+} cells was minimal. Insets on the right show higher magnification of regions outlined in 24-h images. Nuclei stained with DRAQ5 (blue). Images representative of two to three independent experiments. Scale bar, 25 μm.

response to GBS pneumonia is delayed, both in terms of inflammatory mediator production and the accumulation of CD68+ myeloid cells.

We next tested if the delayed inflammatory response in neonates impaired GBS clearance by measuring viable GBS throughout the first 24 h following infection (Figure 2D). In adult lungs, the number of GBS CFU recovered fell steadily over the first 24 h. Juveniles had less dramatic but still significant reductions in CFU by 24 h. However, neonatal mice were not able to reduce GBS CFU counts during the first 24 h following infection, consistent with an inherent defect in killing GBS during the newborn transition. These findings suggested that early in the disease process *in vivo*, neonatal AMΦ lacked the ability to phagocytose and kill GBS. As juvenile mice achieved partial GBS clearance to prevent persistent lung pathology, we more closely examined how long the window of susceptibility to GBS persisted in newborn mice. For these experiments, mice were infected with a higher inoculum of intranasal GBS on days 1, 2, or 3 of life (Figure 2E). Survival depended on day of infection, and 50% of mice infected on day 1 died within the first 24 h. Mice infected on day 2 survived the initial acute period but suffered late mortality between days 11 and 14. In contrast, all mice infected on day 3 of life survived for at least 21 days. When survivors were sacrificed 21 days following infection, we detected significant intrapulmonary GBS only in mice infected on day 1. In subsets of mice infected on day 1 but surviving until day 21, GBS had also spread to the spleen. These findings suggested that mice infected with GBS within the first day of life have reduced survival and lack the ability to adequately clear GBS in the lung and prevent systemic dissemination of the pathogen. Newborn mice apparently acquire the ability to control GBS and protect against devastating infection within the first several days of life.

Confocal microscopy identified potential differences in cellular interactions following GBS infection (Figure 2F). In adult lungs, CD68+ AMΦ localized to the sites of GBS infection within the first 2 h. By 12–24 h, the majority of GBS visualized in adult lungs were inside CD68+ macrophages, consistent with active phagocytosis. These data correlated with CFU kinetics, where the vast majority of viable GBS were cleared from adult lungs within 24 h after infection. In juvenile lungs, AMΦs accumulated around the sites of GBS infection within the first few hours, and some AMΦs were seen to phagocytose GBS. However, by 24 h after infection, substantial quantities of noninternalized GBS were still observed throughout the lung parenchyma, even in areas of AMΦ accumulation. We documented a very different pattern in neonatal lungs. GBS were distributed throughout the lung but also occasionally accumulated in small masses within the airways. AMΦ in these regions surrounded the GBS, but with very little evidence of phagocytic uptake. These data were consistent with CFU data showing lack of significant GBS clearance in neonatal lungs over the first 24 h following infection.

Mature AMΦs Are Required for Rapid GBS Clearance

In the lung, AMΦs provide the major initial response to inhaled or aspirated microbial pathogens. In adults, inflammatory stimuli or lung injury increase expression of CD11b on fully differentiated, Siglec-F+ AMΦs (Duan et al., 2012, 2016). We measured a similar increase in CD11b expression on adult Siglec-F+ AMΦ beginning on the first day after GBS infection with return to baseline levels by day 7 (Figures 3A and S1). Juvenile AMΦ also increased CD11b on day 3 after GBS infection. However, AMΦ in GBS-infected neonatal mice, which did not express Siglec-F until day 3 of life, also did not show a measurable increase in CD11b expression. Therefore, although GBS infection did not interfere with AMΦ acquisition of Siglec-F expression, immature AMΦ within the neonatal lung did not display the same changes in differentiation marker expression as adult cells.

We hypothesized that AMΦ maturity determined either protection against GBS in adults or susceptibility to GBS in neonates. To initially test the requirement of mature AMΦ, we depleted AMΦ from adult mice using liposomal clodronate prior to GBS infection. Intranasal administration of clodronate liposomes reduced the number CD11c+Siglec-F+ AMΦ (Figures 3B and S2). We then infected both clodronate-treated adult mice and controls treated with empty liposomes. By 24 h after GBS infection, confocal imaging of clodronate-treated mice infected with GBS did demonstrate small, CD68lo monocytic cells in the lung after GBS infection, but these cells were not efficient at phagocytosing bacteria (Figure 3C). Clodronate-treated
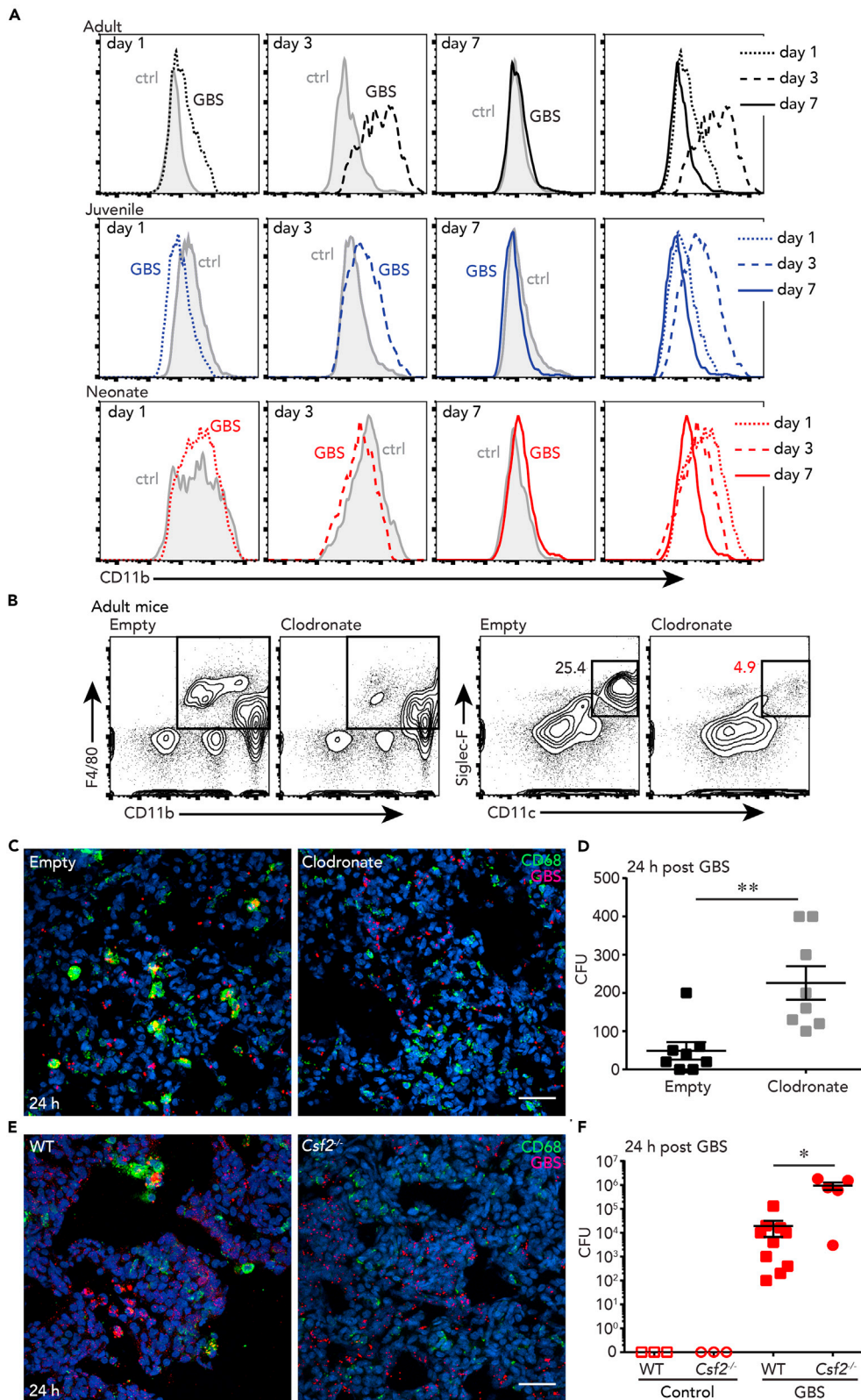
Figure 3. Mature AMΦs Are Required for Rapid GBS Clearance

(A) Flow cytometry of CD11b expression in CD45+CD64+F4/80+ lung macrophages from adult, juvenile, and neonatal mice following GBS infection. In adult mice, GBS increased CD11b expression in Siglec-F+ AMΦs within the first 3 days following infection. Juvenile mice had increased CD11b expression on day 3. However, neonatal lung macrophages did not increase CD11b following GBS infection compared with control, uninfected mice. Data representative of three to four independent experimental replicates.

(B–D) AMΦ depletion using liposomal clodronate reduces GBS killing in adult lungs. (B) Flow cytometry confirming depletion of AMΦs using intranasal liposomal clodronate compared with control mice given empty liposomes. Data representative of two independent experimental replicates. (C) Confocal immunofluorescent micrographs showed GBS persistence (red) in adult mice 24 h after infection (and 72 h after clodronate treatment). Majority of larger CD68+ cells (green) are depleted following liposomal clodronate. Smaller cells expressing lower levels of CD68 likely represent recruited monocytes with reduced capacity to phagocytose GBS. Nuclei counter stained with DRAQ5 (blue). Images taken 24 h after infection Scale bar, 25 μm. (D) Depletion of AMΦs from adult mice reduced GBS killing. CFU recovered from lung 24 h after infection from adults given intranasal clodronate or empty liposomes 48 h prior to infection. Data are represented as mean ± SEM. **p < 0.01 using Mann-Whitney U test (n = 8).

(E and F) Defective GBS killing in neonatal *Csf2*$^{-/-}$ mice. (E) Confocal immunofluorescent micrographs show scattered GBS (red) in *Csf2*$^{-/-}$ mouse lungs 24 h after infection. Scale bar, 25 μm. (F) Neonatal *Csf2*$^{-/-}$ mice had reduced GBS killing 24 h after infection. Data are represented as mean ± SEM. *p < 0.05 using Mann-Whitney U test (n = 5–10). See also Figures S1 and S2.

adults had significantly higher GBS CFU recovered from the lungs compared with control adults (Figure 3D). Consistent with the requirement of AMΦ maturation, newborn *Csf2*−/− mice, which lack fully differentiated AMΦ (Guilliams et al., 2013; Shibata et al., 2001), had higher levels of GBS within their lungs 24 h after infection (Figures 3E and 3F).

Developmental Maturation of Lung Myeloid Siglec Expression

The heavily sialylated capsule of GBS contributes to bacterial virulence. In hosts, the sialic acid-binding immunoglobulin-type lectins Siglec-1 (sialoadhesin, Sn) and Siglec-E both bind GBS sialic acid moieties (Chang et al., 2014a, 2014b). GBS sialic acid binding to Siglec-E reduces the proinflammatory innate immune response to GBS (Chang et al., 2014a). In adult mice, Sn mediates GBS phagocytosis and killing (Chang et al., 2014b). Given the dramatic defects we measured in neonatal mouse lung macrophages, we next examined the developmental dynamics of Siglec-E and Sn expression in lung myeloid populations by FACS (Figure 4; Table S1). In adult lungs, Sn expression was detected in AMΦ (both CD11b^{hi} and CD11b^{lo}) and in recently described CD11c^{neg} nerve and airway-associated macrophages (NAMΦs [Ural et al., 2020]; Figures 4A and S3). Adult neutrophils (PMNs) and interstitial macrophage/monocyte and dendritic cell populations (IM and IM/DC) were Sn-negative. Siglec-E expression was slightly more widespread in adults, being expressed in AMΦs, NAMΦs, neutrophils, and to a lower level in CD11c+ IM/DC cells. Sn and Siglec-E expression in juvenile lung myeloid cells closely resembled the patterns observed in adults (Figure 4B). The neonatal lung contains PMN, IM, and developing AMΦ populations (Figure 4C). Sn expression was only detected in AMΦ, whereas Siglec-E was measured in all populations. Overlaying FACS detection of Sn and Siglec-E in all CD45+ cells (Figures 4D and 4E) and all F4/80+CD11b+ macrophages (Figures 4F and 4G) illustrated the reduced Sn expression in the neonatal lung compared with juveniles and adults. However, expression of the inhibitory Siglec-E was similar across all three timepoints tested.

Developmental Immaturity of AMΦ Siglec-Sialic Acid Detection Contributes to Neonatal GBS Susceptibility

We further investigated the potential contribution of developmental immaturity of Sia receptor expression in neonatal lungs to the inability to rapidly clear GBS. Real-time PCR and immunostaining demonstrated consistently lower Sn expression in newborn mouse lungs (Figures 5A and 5B). We then leveraged a recently completed study examining gene expression in preterm infant tracheal aspirate macrophages to test the dynamics of Sn expression in humans. Samples obtained on the first day of life had lower *hSIGLEC1* (Sn) compared with samples obtained on day 7 (Figure 5C). Expression of *SIGLEC9* (the human paralog of Siglec-E) was similar at these two timepoints. We next tested if deletion of the inhibitory Siglec-E could remove a potential defect in GBS killing. In adult mice (which express high levels of Sn), Siglec-E deletion had no effect on GBS killing (Figures 5D and 5E). However, newborn *SigE*$^{-/-}$ mice showed improved GBS killing compared with WT controls with fewer colonies of bacteria isolated from the lungs 24 h after infection (Figure 5F). Confocal microscopy identified increased GBS phagocytosis in newborn *SigE*$^{-/-}$ lungs compared with controls (Figure 5G). Therefore, removal of the inhibitory Siglec-E improved GBS phagocytosis and killing by neonatal AMΦ even in the setting low Sn expression. In *Csf2*$^{-/-}$ mice that
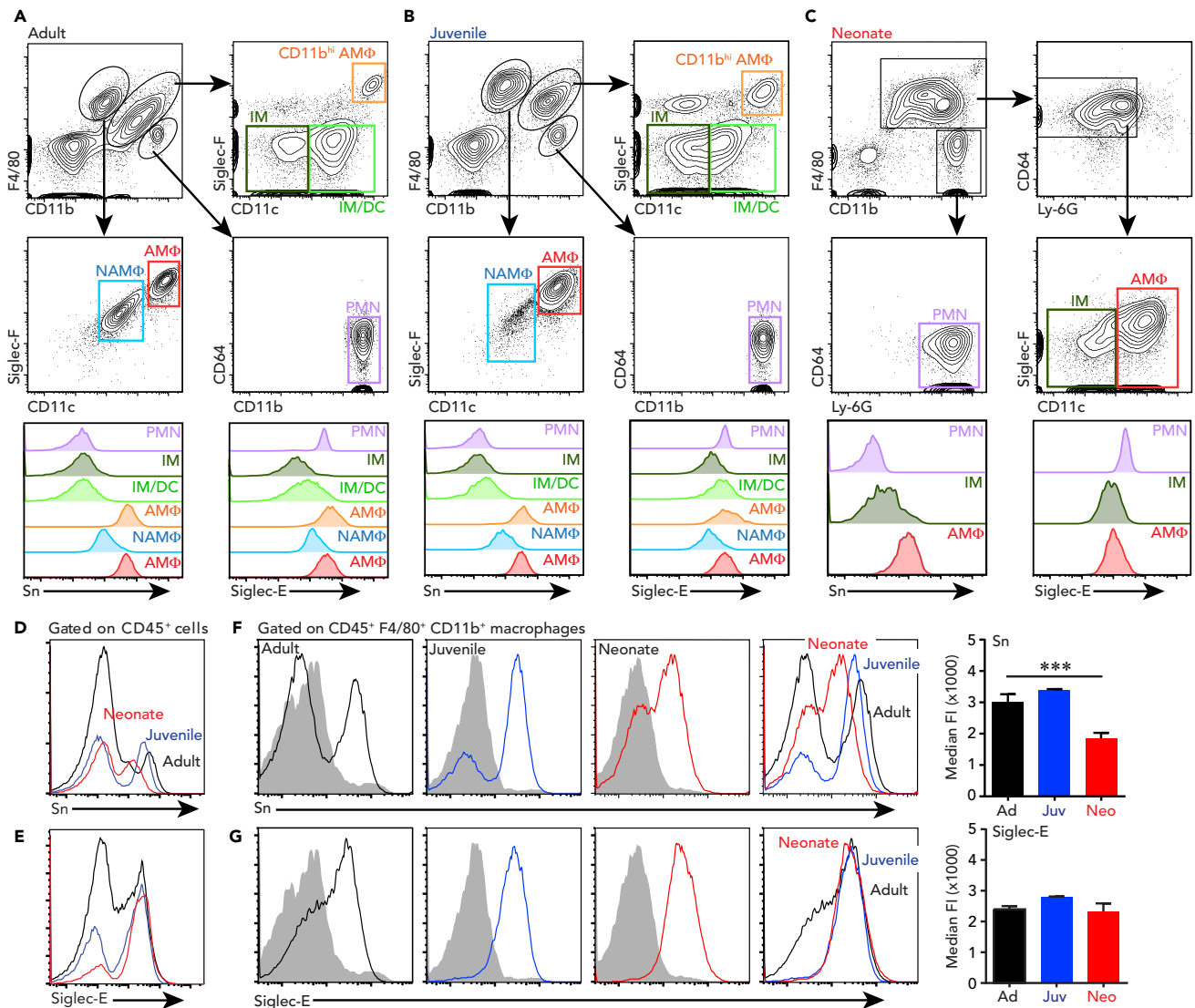
Figure 4. Developmental Maturation of Lung Myeloid Siglec Expression

(A–C) Flow cytometry analysis of Sn and Siglec-E in lung myeloid populations. (A) Gating strategy for CD45$^+$ cells from adult lungs. F4/80^{hi}CD11b^{lo} cells gated on Siglec-F and CD11c to identify AMΦ (Siglec-F$^+$CD11c$^+$) and NAMΦ (CD11c^{lo}). Neutrophils (PMN) identified as F4/80$^-$CD11b$^+$CD64$^-$. The CD11b$^+$F4/80^{lo} population was then gated on Siglec-F and CD11c to identify CD11b$^+$ AMΦ, the CD11c$^+$Siglec-F$^-$ population of interstitial macrophages/monocytes and dendritic cells (IM/DC) and CD11c$^-$Siglec-F$^-$ interstitial macrophages/monocytes (IM). Expression of Sn and Siglec-E are shown below for each myeloid population. (B) Gating strategy for juvenile lungs similar to parameters used for adults. (C) For neonatal lungs, PMNs are identified as CD11b$^+$F4/80$^-$Ly-6G$^+$. Total F4/80$^+$ population then gated on CD64$^+$Ly-6G$^-$ cells, followed by Siglec-F and CD11c to identify Siglec-F$^-$CD11c$^-$ IM and CD11c$^+$ AMΦ, including immature and developing AMΦ populations.

(D and E) Developmental changes in Sn and Siglec-E expression in lung immune cells as measured by flow cytometry. Sn and Siglec-E expression plotted for entire CD45$^+$ lung populations from adult, juvenile, and neonatal mice.

(F and G) Developmental changes in Sn and Siglec-E within lung macrophages. Sn and Siglec-E expression measured by flow cytometry and plotted for CD45$^+$F4/80$^+$CD11b$^+$ total macrophage populations from adult, juvenile, and neonatal mice. Gray shaded peak is the isotype control for each sample. Right panels show Median Fluorescent Intensity of Sn and Siglec-E in total macrophage populations. Data are represented as mean ± SEM. ***p < 0.001 using Mann-Whitney U test (n = 3–8). See also Figures S2 and S3, and Table S1.

lack normal AMΦ differentiation, we detected even lower neonatal Sn expression on lung macrophages compared with WT neonatal mice (Figure 5H). Adult *Csf2$^{-/-}$* AMΦ lacked Siglec-E expression, whereas expression in neonates was similar (Figure 5I). Therefore, in both mice and humans, immature newborn AMΦ have adult levels of the inhibitory receptor Siglec-E but lack expression of Sn. Alterations of the
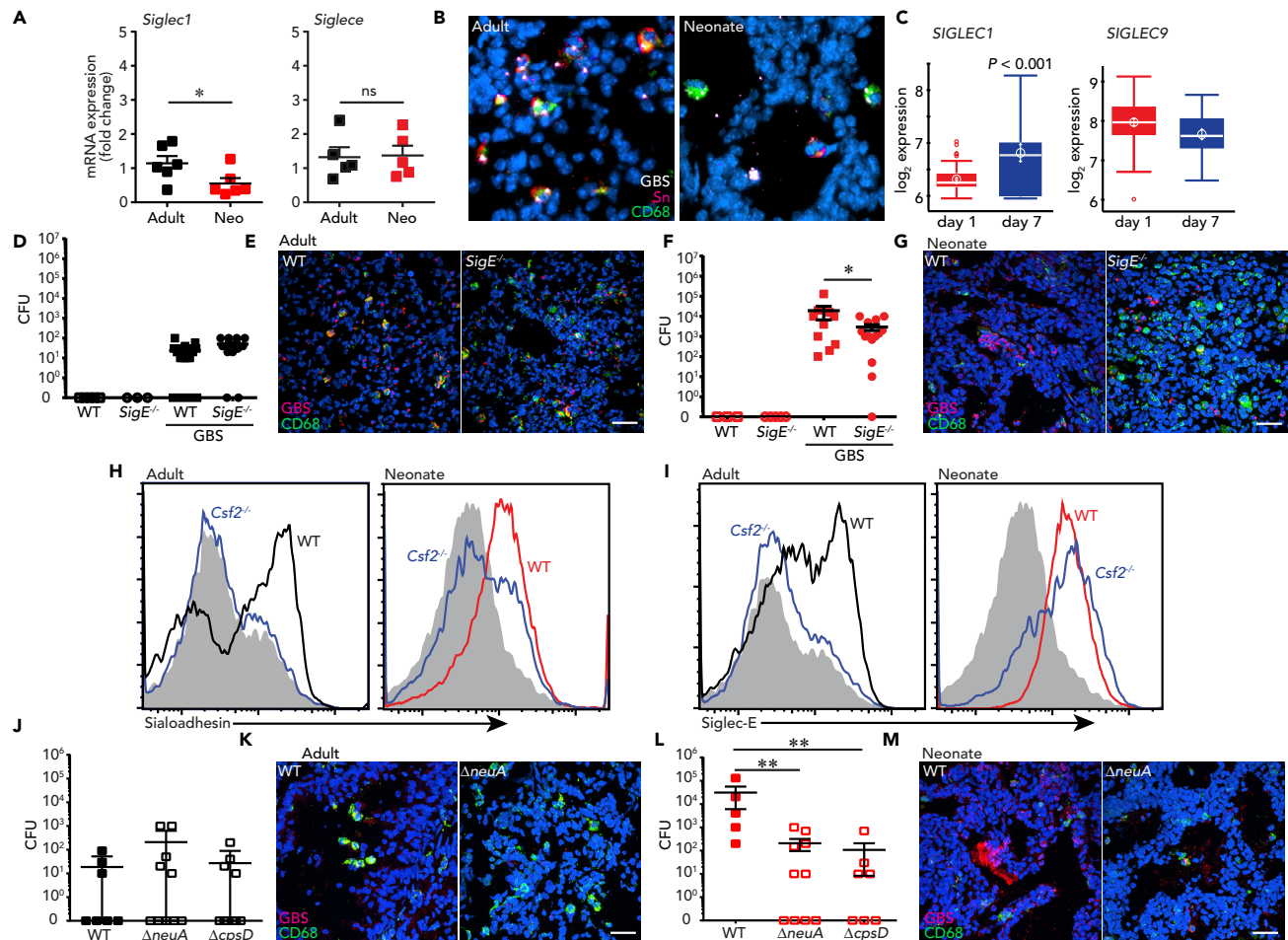
Figure 5. Developmental Immaturity of AMΦ Siglec-Sialic Acid Detection Contributes to Neonatal GBS Susceptibility

(A) Neonatal lungs had reduced *Siglec1* mRNA expression compared with adults but similar levels of *Siglece*. Normalized to *Gapdh* and represented as fold change compared with adult samples. Data are represented as mean ± SEM. Significance calculated using ΔC$_T$ values. * = p < 0.05, using unpaired t test. (n = 4–6 mice per time point).

(B) Confocal immunofluorescent micrographs showing extensive Sialoadhesin expression (red) in adult CD68+ macrophages following GBS infection (left panel). Presence of Sialoadhesin-expressing cells was reduced in neonatal lungs (right panel). Images taken 24 h after infection.

(C) Human *SIGLEC1* and *SIGLEC9* (human *Siglece* paralog) gene expression in lung macrophages obtained from human preterm newborns on day 1 and day 7 of life showing reduced *SIGLEC1* expression at birth with increased levels by 1 week of age. *SIGLEC9* expression was unchanged. Expression measured by Affymetrix GeneChip Human Transcriptome 2.0 arrays. Boxplots are shown with mean as circle with arrows representing ±SD, median as white line with 95% confidence intervals as colored lines (n = 83 on day 1, n = 46 on day 7).

(D and E) Siglec-E is not required for GBS killing in adult mice. (D) Similar CFU recovered from WT and *SigE*$^{-/-}$ adult mouse lungs 24 h after GBS infection (n = 11–15). Data are represented as mean ± SEM. (E) Confocal immunofluorescent micrographs showed similar patterns of CD68 (green) and GBS (red) in WT and *SigE*$^{-/-}$ adult lungs 24 h after infection. Images are representative of three independent experimental replicates. Scale bar, 25 μm.

(F and G) GBS killing is increased in neonatal *SigE*$^{-/-}$ mice. (F) Compared with WT controls, neonatal *SigE*$^{-/-}$ mice had reduced CFU recovered from lung 24 h after GBS infection. Data are represented as mean ± SEM. **p < 0.005 using Mann-Whitney U test (n = 10 for WT, n = 24 for *SigE*$^{-/-}$). (G) Confocal immunofluorescent micrographs demonstrated reduced GBS overall (red) and increased GBS phagocytosis by CD68$^+$ cells in *SigE*$^{-/-}$ neonatal mouse lungs 24 h after infection. Images are representative of three independent experimental replicates. Scale bar, 25 μm.

(H) Flow cytometry showing reduced Sialoadhesin expression in both adult and neonatal lung macrophages from *Csf2*$^{-/-}$ mice. Data are representative of two independent experimental replicates.

(I) Siglec-E expression in AMΦ was reduced in adult *Csf2*$^{-/-}$ mice compared with WT controls (left panel) but similar in neonatal *Csf2*$^{-/-}$ lung macrophages (right panel). Data are representative of two independent experimental replicates.

(J) Killing of WT, *ΔneuA*, or *ΔcpsD* GBS was similar in adult mice 24 h after intranasal infection (n = 7–10). Data are represented as mean ± SEM.

(K) Confocal immunofluorescent micrographs showed only rare GBS staining (red) in adult mice 24 h after infection with either WT GBS or *ΔneuA* GBS. Images are representative of two to three independent experimental replicates. Scale bar, 25 μm.

(L) Neonatal mice had increased ability to kill GBS with defects in sialic acid capsule synthesis. CFU measured 24 h after infection. Data are represented as mean ± SEM. **p < 0.01 using Mann-Whitney U test (n = 7–10).

(M) Confocal immunofluorescent micrographs showed increased *ΔneuA* GBS (red) phagocytosis by CD68$^+$ macrophages (green) 24 h after infection. Images are representative of two to three independent experimental replicates.

GBS capsule to eliminate sialic acid also improved clearance in the neonatal lung. We infected mice with GBS strains bearing mutations in genes critical for either sialic acid modification (Δ*neuA*) or capsule formation (Δ*cpsD*). Although clearance in adults was similar to WT GBS (Figures 5J and 5K), newborn mice showed improved phagocytosis and killing of both Δ*neuA* and Δ*cpsD* strains (Figures 5L and 5M), confirming that the sialic acid-rich GBS capsule is a key virulence factor in the neonatal lung.

DISCUSSION

We corroborated the unique susceptibility of newborns to GBS pneumonia using a novel murine model. Similar to the pathogenesis of GBS pneumonia in human newborns, infected neonatal mice fail to clear intrapulmonary GBS, develop persistent lung injury, and suffer increased mortality compared with older mice and adults. The window of susceptibility appears restricted to the newborn period, since even 2- to 3-day-old mice have much better outcomes compared with mice infected on the first day of life. As in humans, adult mice are resistant to GBS lung infection, quickly clearing bacteria within the lung and completely resolving any signs of lung injury or pathology. Interestingly, the primary immune defect in newborn mice may lie in the inability of AMΦs to effectively phagocytose and kill GBS within the lung. GBS persisted in a subpopulation of animals infected at birth, leading to bacteremia, and spread to the central nervous system. Neonatal mice did, however, mount an inflammatory immune response to GBS, albeit with altered kinetics compared with juvenile and adult animals. In addition to a delayed initiation of lung inflammation, neonatal mice had persistent lung injury up to 1 week after infection. Although many functional aspects of the lung immune system may be underdeveloped at birth, our data point to immaturity of lung AMΦs as particularly important in rendering the newborn susceptible to disease.

Like many human pathogens, GBS expresses a variety of virulence factors to subvert host immune detection and killing and/or promote cellular damage (Bebien et al., 2012; Doran et al., 2002). However, the same GBS strains that asymptomatically colonize adults can cause devastating disease in newborns. We hypothesized that the neonatal window of susceptibility is primarily due to defective maturation of host pulmonary innate immunity. In addition to AMΦ function, lung immunity includes antimicrobial peptides, surfactant, mechanical mucus clearance, resident lymphocyte and dendritic cell function, and neutrophil influx (Evans et al., 2010; Lambert and Culley, 2017; Nicod, 2005). Although our data here do not discount important contributions of these or any other mechanisms, rapid GBS clearance was impaired in mice depleted of AMΦs and in *Csf2*⁻/⁻ mice that lack mature AMΦs. Our data also clearly demonstrated that neonatal AMΦs lack sufficient expression of Sn for effective detection, phagocytosis, and killing of sialylated GBS. We propose that this neonatal immaturity might allow persistent GBS lung infection in some newborns, significantly increasing the risk of systemic spread to produce bacteremia, sepsis, and meningitis.

Multiple immune cell populations within the lung respond to serious bacterial infection and likely contribute to the subsequent repair process. Developmental immaturity of these cell populations therefore contributes to infectious disease risk and pathogenesis in newborns. Our data reinforce the paradigm of incomplete lung myeloid cell differentiation at birth with identification of key contributing lectin-glycan interactions and associated receptor signaling pathways. Sn-expressing NAMΦ populations were present at low numbers in juvenile mice and not detected in newborns. Different populations of IM and DC were also difficult to identify in newborn mouse lungs, potentially owing to their incomplete differentiation. Although we conclude that neonatal GBS susceptibility is significantly impacted by AMΦ immaturity, additional immune development defects also make the newborn particularly vulnerable.

Our findings suggest potential new opportunities for protecting newborns from infection. In addition to antimicrobial treatment of both mothers and newborns at risk of serious infection (Boyer and Gotoff, 1986), strategies aimed at improving or accelerating AMΦ maturation could provide protection against GBS. Specifically, identifying ways to improve GBS killing by the immature AMΦs found in the newborn lung could mitigate against both early-onset pneumonia and the risk of late-onset sepsis and meningitis. The inflammatory response in adult and newborn lungs also appears to follow a very different time course after GBS infection. AMΦs detect GBS via multiple pattern recognition receptors, including the TLR family members TLR2, TLR6, TLR7, TLR8/13, and TLR9 (Henneke et al., 2001, 2002; Talati et al., 2008). Importantly, both neonatal and adult AMΦs expressed Siglec-E, which engages the repeated α2-3 sialic acid motif of the GBS capsule and attenuates innate immune signaling via SHP-1/2-mediated TBK1 inhibition (Chang et al., 2014a). Therefore, neonatal Siglec-E expression may suppress GBS-mediated immune signaling and cytokine production until other pathways are engaged or Sn expression increases. As pro-inflammatory signals are also required for initiating an anti-inflammatory host response, additional experimental

studies will be required to determine if targeting specific components of immune signaling will prove beneficial or harmful in the setting of neonatal GBS infection. Murine experimental models like the one developed here may therefore prove invaluable for testing potential therapeutic strategies and interventions.

Limitations of the Study

In humans, newborns first encounter GBS either through ascending infection following amniotic membrane rupture or aspiration of GBS during the birth process. Although GBS colonization of the maternal urinary tract and vaginal canal have been modeled in mice (Andrade et al., 2018), direct inoculation of mice with defined and consistent numbers of GBS allowed us to test the relative impact of infection on the first day of life and during the postnatal period. We expected some variability in any pneumonia model, especially when using a noninvasive approach to infect newborn mice. However, our data support the use of this model in reliably and reproducibly modeling neonatal infection. Given these potential caveats, our data strongly support the primary role of AMΦs in providing immunity against GBS in adult lungs and demonstrate how AMΦ immaturity leads to defects in GBS clearance.

Resource Availability

Lead Contact

Further information and requests for resources and reagents should be directed to and will be fulfilled by the Lead Contact, Lawrence S. Prince (lprinceucsd@gmail.com).

Materials Availability

Mouse strains used in this study are available from Jackson Laboratories and Envigo. Unique bacterial strains and reagents used in this study are available from the Lead Contact and may require a Materials Transfer Agreement.

Data and Code Availability

The human preterm infant lung macrophage dataset included in Figure 5 is available through the Gene Expression Omnibus (GSE149490).

METHODS

All methods can be found in the accompanying Transparent Methods supplemental file.

SUPPLEMENTAL INFORMATION

Supplemental Information can be found online at https://doi.org/10.1016/j.isci.2020.101207.

AUTHOR CONTRIBUTIONS

Conceptualization, S.J.L., V.N., L.S.P.; Methodology, S.J.L., K.A.P., V.N., L.S.P.; Investigation, S.J.L., K.A.P., J.M.K., A.Y., L.D.B., P.G.B.D.R., G.E.H., A.M.M., O.L.; Writing – Original Draft, S.J.L., L.S.P.; Writing – Review & Editing, All authors; Funding Acquisition, V.N., L.S.P.; Resources, V.N., L.S.P.

DECLARATION OF INTERESTS

The authors declare no competing interests with the results of this study.

REFERENCES

Allard, B., Panariti, A., and Martin, J.G. (2018). Alveolar macrophages in the resolution of inflammation, tissue repair, and tolerance to infection. Front. Immunol. 9, 1777.

Andrade, E.B., Magalhaes, A., Puga, A., Costa, M., Bravo, J., Portugal, C.C., Ribeiro, A., Correia-Neves, M., Faustino, A., Firon, A., et al. (2018). A mouse model reproducing the pathophysiology of neonatal group B streptococcal infection. Nat. Commun. 9, 3138.

Baker, C.J., and Barrett, F.F. (1973). Transmission of group B streptococci among parturient women and their neonates. J. Pediatr. 83, 919–925.

Bebien, M., Hensler, M.E., Davanture, S., Hsu, L.-C., Karin, M., Park, J.M., Alexopoulou, L., Liu, G.Y., Nizet, V., and Lawrence, T. (2012). The pore-forming toxin β hemolysin/cytolysin triggers p38 MAPK-dependent IL-10 production in macrophages and inhibits innate immunity. PLoS Pathog. 8, e1002812.

Berclaz, P.-Y., Shibata, Y., Whitsett, J.A., and Trapnell, B.C. (2002). GM-CSF, via PU.1, regulates alveolar macrophage FcγR-mediated phagocytosis and the IL-18/IFN-γ–mediated molecular connection between innate and adaptive immunity in the lung. Blood 100, 4193–4200.

Boyer, K.M., and Gotoff, S.P. (1986). Prevention of early-onset neonatal group B streptococcal disease with selective intrapartum chemoprophylaxis. N. Engl. J. Med. 314, 1665–1669.

Byrne, A.J., Mathie, S.A., Gregory, L.G., and Lloyd, C.M. (2015). Pulmonary macrophages: key players in the innate defence of the airways. Thorax 70, 1189–1196.

Chang, Y.-C., Olson, J., Beasley, F.C., Tung, C., Zhang, J., Crocker, P.R., Varki, A., and Nizet, V. (2014a). Group B Streptococcus engages an inhibitory Siglec through sialic acid mimicry to blunt innate immune and inflammatory responses in vivo. PLoS Pathog. 10, e1003846.

Chang, Y.-C., Olson, J., Louie, A., Crocker, P.R., Varki, A., and Nizet, V. (2014b). Role of macrophage sialoadhesin in host defense against the sialylated pathogen group B Streptococcus. J. Mol. Med. 92, 951–959.

Doran, K.S., Chang, J.C., Benoit, V.M., Eckmann, L., and Nizet, V. (2002). Group B streptococcal beta-hemolysin/cytolysin promotes invasion of human lung epithelial cells and the release of interleukin-8. J. Infect. Dis. 185, 196–203.

Duan, M., Li, W.C., Vlahos, R., Maxwell, M.J., Anderson, G.P., and Hibbs, M.L. (2012). Distinct macrophage subpopulations characterize acute infection and chronic inflammatory lung disease. J. Immunol. 189, 946–955.

Duan, M., Steinfort, D.P., Smallwood, D., Hew, M., Chen, W., Ernst, M., Irving, L.B., Anderson, G.P., and Hibbs, M.L. (2016). CD11b immunophenotyping identifies inflammatory

profiles in the mouse and human lungs. Mucosal Immunol. 9, 550–563.

Evans, S.E., Xu, Y., Tuvim, M.J., and Dickey, B.F. (2010). Inducible innate resistance of lung epithelium to infection. Annu. Rev. Physiol. 72, 413–435.

Fliegauf, M., Sonnen, A.F.P., Kremer, B., and Henneke, P. (2013). Mucociliary clearance defects in a murine in vitro model of pneumococcal airway infection. PLoS One 8, e59925.

Franciosi, R.A., Knostman, J.D., and Zimmerman, R.A. (1973). Group B streptococcal neonatal and infant infections. J. Pediatr. 82, 707–718.

Guilliams, M., De Kleer, I., Henri, S., Post, S., Vanhoutte, L., De Prijck, S., Deswarte, K., Malissen, B., Hammad, H., and Lambrecht, B.N. (2013). Alveolar macrophages develop from fetal monocytes that differentiate into long-lived cells in the first week of life via GM-CSF. J. Exp. Med. 210, 1977–1992.

Henneke, P., Takeuchi, O., Malley, R., Lien, E., Ingalls, R.R., Freeman, M.W., Mayadas, T., Nizet, V., Akira, S., Kasper, D.L., et al. (2002). Cellular activation, phagocytosis, and bactericidal activity against group B Streptococcus involve parallel myeloid differentiation factor 88-dependent and independent signaling pathways. J. Immunol. 169, 3970–3977.

Henneke, P., Takeuchi, O., van Strijp, J.A., Guttormsen, H.K., Smith, J.A., Schromm, A.B., Espevik, T.A., Akira, S., Nizet, V., Kasper, D.L., et al. (2001). Novel engagement of CD14 and multiple Toll-like receptors by group B streptococci. J. Immunol. 167, 7069–7076.

Horn, K.A., Meyer, W.T., Wyrick, B.C., and Zimmerman, R.A. (1974). Group B streptococcal neonatal infection. JAMA 230, 1165–1167.

Kopf, M., Schneider, C., and Nobs, S.P. (2015). The development and function of lung-resident macrophages and dendritic cells. Nat. Immunol. 16, 36.

Lambert, L., and Culley, F.J. (2017). Innate immunity to respiratory infection in early life. Front. Immunol. 8, 1570.

Madrid, L., Seale, A.C., Kohli-Lynch, M., Edmond, K.M., Lawn, J.E., Heath, P.T., Madhi, S.A., Baker, C.J., Bartlett, L., Cutland, C., et al. (2017). Infant group B streptococcal disease incidence and serotypes worldwide: systematic Review and meta-analyses. Clin. Infect. Dis. 65, S160–S172.

Nicod, L.P. (2005). Lung defences: an overview. Eur. Respir. Rev. 14, 45–50.

Pitts, S.I., Maruthur, N.M., Langley, G.E., Pondo, T., Shutt, K.A., Hollick, R., Schrag, S.J., Thomas, A., Nichols, M., Farley, M., et al. (2018). Obesity, diabetes, and the risk of invasive group B streptococcal disease in nonpregnant adults in the United States. Open Forum Infect. Dis. 5, ofy030.

Raabe, V.N., and Shane, A.L. (2019). Group B Streptococcus (Streptococcus agalactiae). Microbiol. Spectr. 7, 3–5.

Randis, T.M., Baker, J.A., and Ratner, A.J. (2017). Group B streptococcal infections. Pediatr. Rev. 38, 254–262.

Russell, N.J., Seale, A.C., O'Sullivan, C., Le Doare, K., Heath, P.T., Lawn, J.E., Bartlett, L., Cutland, C., Gravett, M., Ip, M., et al. (2017). Risk of early-onset neonatal group B streptococcal disease with maternal colonization worldwide: systematic Review and meta-analyses. Clin. Infect. Dis. 65, S152–S159.

Schneider, C., Nobs, S.P., Kurrer, M., Rehrauer, H., Thiele, C., and Kopf, M. (2014). Induction of the nuclear receptor PPAR-gamma by the cytokine GM-CSF is critical for the differentiation of fetal monocytes into alveolar macrophages. Nat. Immunol. 15, 1026–1037.

Seale, A.C., Bianchi-Jassir, F., Russell, N.J., Kohli-Lynch, M., Tann, C.J., Hall, J., Madrid, L., Blencowe, H., Cousens, S., Baker, C.J., et al. (2017). Estimates of the burden of group B streptococcal disease worldwide for pregnant women, stillbirths, and children. Clin. Infect. Dis. 65, S200–S219.

Shibata, Y., Berclaz, P.-Y., Chroneos, Z.C., Yoshida, M., Whitsett, J.A., and Trapnell, B.C. (2001). GM-CSF regulates alveolar macrophage differentiation and innate immunity in the lung through PU.1. Immunity 15, 557–567.

Skoff, T.H., Farley, M.M., Petit, S., Craig, A.S., Schaffner, W., Gershman, K., Harrison, L.H., Lynfield, R., Mohle-Boetani, J., Zansky, S., et al. (2009). Increasing burden of invasive group B streptococcal disease in nonpregnant adults, 1990-2007. Clin. Infect. Dis. 49, 85–92.

Talati, A.J., Kim, H.J., Kim, Y.I., Yi, A.K., and English, B.K. (2008). Role of bacterial DNA in macrophage activation by group B streptococci. Microbes Infect. 10, 1106–1113.

Ural, B.B., Yeung, S.T., Damani-Yokota, P., Devlin, J.C., de Vries, M., Vera-Licona, P., Samji, T., Sawai, C.M., Jang, G., Perez, O.A., et al. (2020). Identification of a nerve-associated, lung-resident interstitial macrophage subset with distinct localization and immunoregulatory properties. Sci. Immunol. 5, https://doi.org/10.1126/sciimmunol.aax8756.

Weitnauer, M., Mijosek, V., and Dalpke, A.H. (2016). Control of local immunity by airway epithelial cells. Mucosal Immunol. 9, 287–298.

Whitsett, J.A., and Alenghat, T. (2015). Respiratory epithelial cells orchestrate pulmonary innate immunity. Nat. Immunol. 16, 27–35.

Yu, X., Buttgereit, A., Lelios, I., Utz, S.G., Cansever, D., Becher, B., and Greter, M. (2017). The cytokine TGF-beta promotes the development and homeostasis of alveolar macrophages. Immunity 47, 903–912.e4.

Supplemental Information

Developmental Immaturity of Siglec Receptor Expression

on Neonatal Alveolar Macrophages Predisposes

to Severe Group B Streptococcal Infection

Sean J. Lund, Kathryn A. Patras, Jacqueline M. Kimmey, Asami Yamamura, Lindsay D. Butcher, Pamela G.B. Del Rosario, Gilberto E. Hernandez, Alyssa M. McCoy, Omar Lakhdari, Victor Nizet, and Lawrence S. Prince
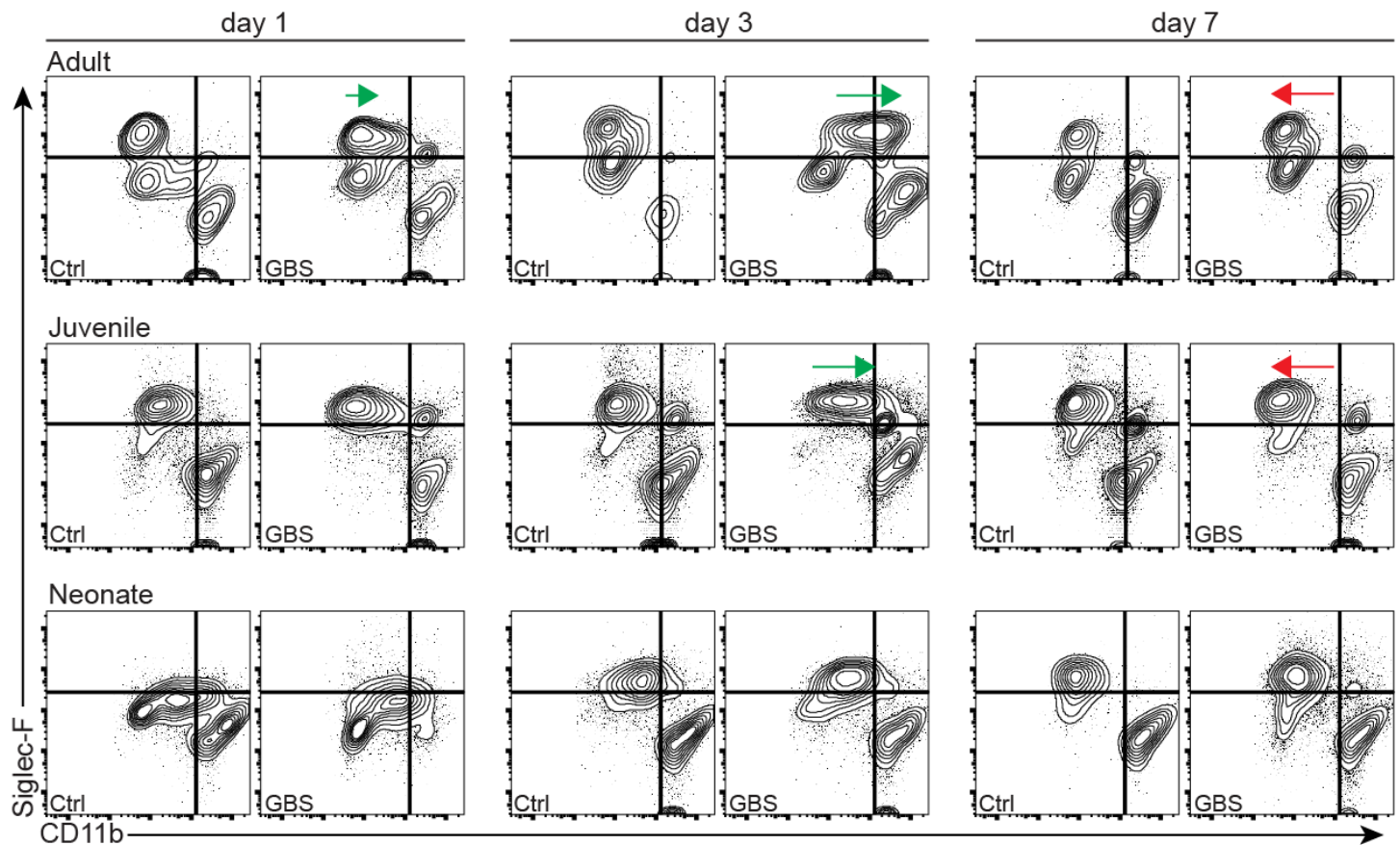
Figure S1 (Refers to Figure 3). Changes in macrophage marker expression following GBS infection. FACS data showed increased CD11b expression in adult AMΦ following GBS infection with resolution by day 7. Juvenile mice showed similar if less obvious increase in CD11b expression. In contrast, neonatal lung macrophages continued the normal developmental transition to express Siglec-F following GBS infection without any measurable changes in CD11b expression. Arrows represent changes in population relative to control.
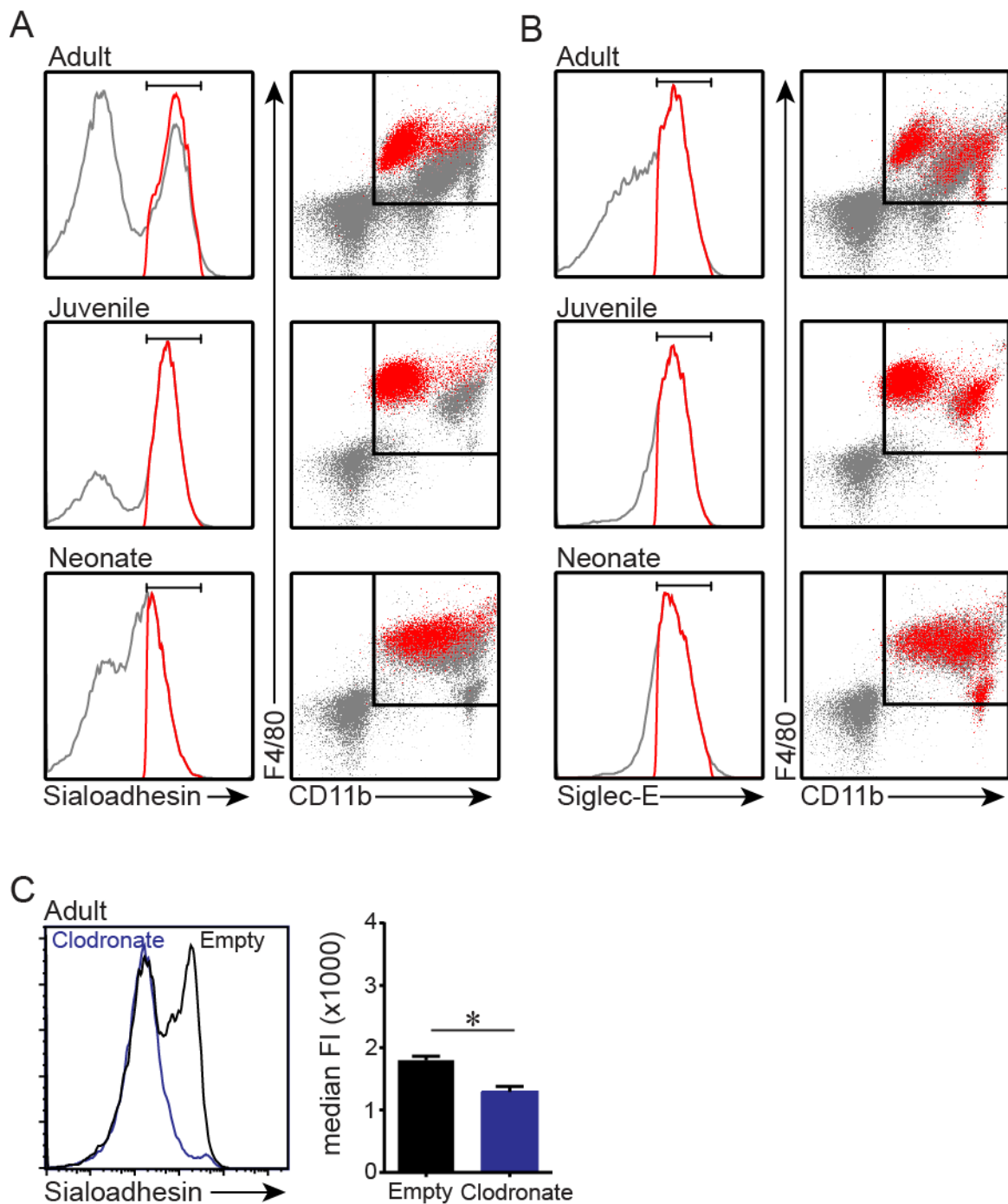
Figure S2 (Refers to Figures 3,4). Sialoadhesin and Siglec-E receptor expression in lung macrophage populations. (A) Backgating analysis of Sialoadhesin expressing cells seen in adult and juvenile mice and extrapolated to neonates. Sialoadhesin expression restricted to AMΦ populations in adult and juvenile mice and pre-alveolar macrophages in neonates. (B) Backgating analysis of Siglec-E expression shows both alveolar and interstitial lung macrophage populations express Siglec-E. (C) Intranasal liposomal clodronate depleted the adult lung of Sialoadhesin-expressing macrophages consistent with restriction to AMΦ populations. Control animals were given empty liposomes for comparison. Error bars represent S.E.M. * $P < 0.05$, n = 4.
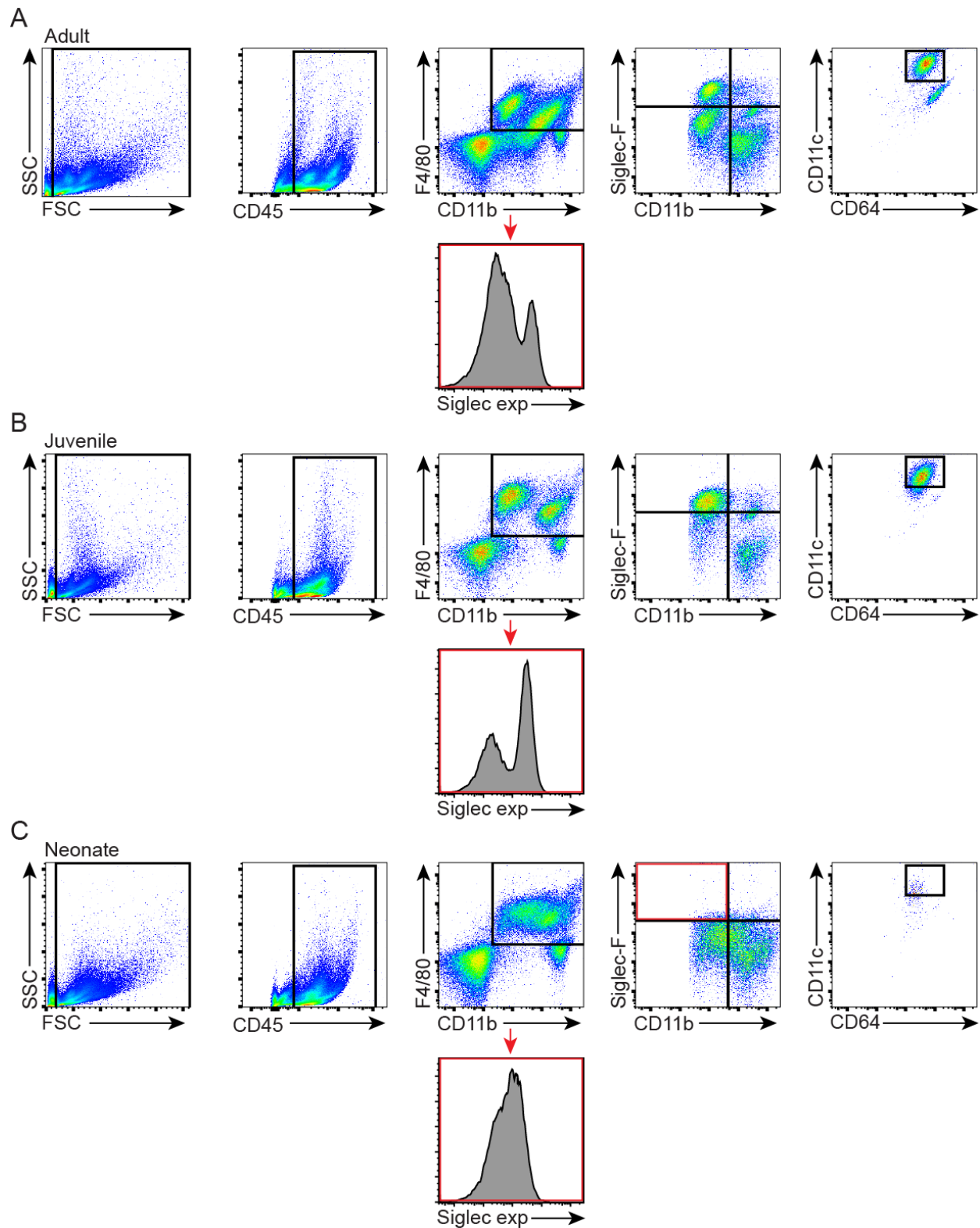
Figure S3 (Refers to Figure 4). Gating strategy for measuring Siglec receptor expression on lung macrophage populations. **(A-C)** Gating strategy used for analyzing macrophages throughout the paper and Siglec receptor expression in Figure 4. CD45+F4/80+CD11b+/- macrophages were analyzed across all developmental timepoints. Importantly, Siglec-F expression occurs during the first week of postnatal life and is therefore absent in neonatal lung pre-alveolar macrophages.

AMΦ	CD45$^+$F4/80^{hi}CD11b^{lo}CD11c$^+$Siglec-F$^+$
CD11b$^+$ AMΦ	CD45$^+$F4/80^{hi}CD11b^{hi}CD11c$^+$Siglec-F$^+$
NAMΦ	CD45$^+$F4/80^{hi}CD11b^{lo}CD11c^{lo}Siglec-F^{lo}
CD11c$^-$ IM	CD45$^+$F4/80^{lo}CD11b^{hi}CD11c$^-$Siglec-F$^-$
CD11c$^+$ IM/DC	CD45$^+$F4/80^{lo}CD11b^{hi}CD11c$^+$Siglec-F$^-$
PMN	CD45$^+$F4/80$^-$CD11b^{hi}CD64$^-$

Supplemental Table S1 (Gating strategy for lung myeloid cell populations in Figure 4).

Transparent Methods

Mice
Wild-type (WT) male and female C57BL/6 mice were obtained from Envigo and bred in house. Adult (8-10 weeks of age), juvenile (postnatal day 7, PND7), and neonatal (PND1, PND2, or PND3) were used. All animal experiments, including infections, were approved the University of California, San Diego Institutional Animal Care and Use Committee (IACUC). After infections, mice were monitored twice daily. Any mouse that lost >10% body weight or exhibited signs of severe disease or distress was humanely euthanized prior to the defined endpoint of the experiment.

Bacteria
The WT GBS strain used in all experiments was COH1, a highly encapsulated serotype III clinical isolate (Wessels et al., 1991) with established virulence in murine models of pneumonia, sepsis and meningitis (Chang et al., 2014; Doran et al., 2003; Hensler et al., 2008). All strains were propagated in Todd-Hewitt Broth (THB). COH1 was transformed with a GFP expression plasmid (erythromycin selection) to enable easier detection in the earlier time point pneumonia challenge studies. Isogenic, in frame allelic replacement mutants in the COH1 background lacking its capsular polysaccharide (ΔcpsD, aka HY106) or only the terminal sialic acid of the capsule side chain (ΔneuA) were also used, and their generation has been previously described (Lewis et al., 2004; Yim et al., 1997).

Pneumonia Model
Adult, juvenile, and neonatal mice were infected with a weight-adjusted inoculum of GBS so that immune responses could be compared between age groups. WT GBS (strain COH1) was used in the longer time points model (1, 3, and 7 days). A GFP-expressing GBS (strain COH1) was used in the shorter time points model (0.5, 2, 6, 12, 24 h). Neonatal mice (PND1-PND3) were also infected with a larger inoculum, 100x more concentrated than the standard inoculum used. Survival was monitored over the course of 21 days and any animal showing signs of severe disease was humanely euthanized. An overnight culture of GBS in THB was sub-cultured and grown to mid-logarithmic phage (OD_{600} = 0.4). One ml of sub cultured GBS was then removed and washed with HBSS, centrifuged for 5 min at 5,000 RPM, the bacterial pellet resuspended in 1 ml HBSS, and serial dilutions performed to the desired inoculum. Due to the differing volumes of air space in the lungs between adults, juveniles, and neonates, in order to give equivalent doses of GBS to each age group the volume of the intranasal inoculum had to be adjusted. Adults were given 50 µl of GBS suspension intranasally, juveniles 10 µl, and neonates 2 µl. Adults weighed, on average, 5-fold times more than juveniles, and 25-fold more than neonates. Adults, juveniles, and neonates were anesthetized using 3% isoflurane. The corresponding amount of GBS suspension was then pipetted into the nares and aspirated. Animals were monitored until recovery from anesthesia.

Bacterial Quantification
Bacterial counts were obtained by homogenizing the medial and caudal lobes of the lung in 1 ml HBSS. The resultant lung homogenate and serial 10-fold dilutions were plated on Todd-Hewitt agar (THA) plates, which were incubated at 37°C for 24 h, at which point colony forming units (CFU) were enumerated.

Histology
The right lobes of the lung in adults, juveniles, and neonates were removed and fixed in 4% paraformaldehyde overnight. The following day, lung lobes were dehydrated via changes along an ethanol gradient. Paraffin embedding, sectioning, and hematoxylin and eosin (H&E) staining were all performed by the UC San Diego Histology Core at the Moores Cancer Center. Hematoxylin and eosin (H&E)-stained micrographs were captured using a Leica brightfield microscope and color CCD camera.

Lung Pathology Scoring
Adult, juvenile, and neonatal H&E stained micrographs were analyzed for interstitial inflammation, alveolar inflammation, alveolar collapse, bronchitis, and endothelitis. Each category was scored 0-3 (absent, mild, moderate, severe) by 3 blinded independent reviewers. The scores were compiled and statistical analysis performed as below.

Flow Cytometry

The left lobes of adult, juvenile, and neonatal mice were processed and digested in RPMI containing 2 mg/mL of collagenase IV for 15 min. The resulting single-cell suspension was filtered and washed. Lung cells were stained with CD45 (BD Biosciences), CD11b (BioLegend), CD11c (BioLegend), CD64 (BioLegend), F4/80 (BioLegend), Siglec-F (BD Biosciences), Gr-1 (BioLegend), and MHC-II (BioLegend), Siglec-E (BioLegend), CD169/Sialoadhesin (BioLegend) for 30 min at 4°C. Cells were then washed and resuspended in FACS buffer. The cells were analyzed by flow cytometry on a BD FacsCanto II using FlowJo software.

RNA Extraction and cDNA synthesis
The cranial and accessory lobes of adult, juvenile, and neonatal lungs were snap frozen in a bath of ethanol and dry ice for later RNA extraction. For extraction, the snap frozen lungs were suspended in 500 µl TRIzol reagent (Ambion) and homogenized using mechanical pestle motor. An additional 500 µl TRIzol was added and the homogenate kept at room temperature for 5 min prior to addition of chloroform for extraction of RNA. There, the upper aqueous layer was washed with isopropanol and ethanol, and RNA suspended in molecular grade water for quantification on a NanoDrop spectrophotometer. cDNA synthesis was performed using a Superscript III Reverse Transcription Kit (Invitrogen) according to the manufacturer's protocol.

qPCR
qPCR reactions were run on a BioRad CFX96 Touch Real-time System for 40 cycles. Briefly, each reaction consisted of 16 µl of SYBR green (BioRad), 9.44 microliters of µl grade H_2O, 6.4 microliters of forward and reverse primers (sequences listed below, Integrated DNA Technologies), and 0.16 microliters of cDNA. Each reaction was added in triplicate, 10 µl per well.

Gene	Forward (5' - 3')	Reverse (5' - 3')
Gapdh	AGTATGACTCCACTCACGGC	CACCAGTAGACTCCACGACA
Il1b	GGAGAACCAAGCAACGACAAAATA	TGGGGAACTCTGCAGACTCAAAC
Il6	AAACCGCTATGAAGTTCCTCTCTG	ATCCTCTGTGAAGTCTCCTCTCC
Cxcl1	CAGCCACCCGCTCGCTTCTC	TCAAGGCAAGCCTCGCGACCAT
Siglec1	GCTGGTGGACAAGCGTTTC	TTCAAGTCTTTGAGCAACAGGT
Siglece	GTCTCCACAGAGCAGTGCAACTTTATC	TGGGATTCAACCAGGGGATTCTGAG

Immunofluorescence and Confocal microscopy
The left lobes of adult, juvenile, and neonatal mice were removed and briefly fixed in 4% paraformaldehyde for 1 h at room temperature. Following fixation, lungs were washed in PBS containing Ca^{2+} and Mg^{2+} and put in 15% sucrose until they sank to the bottom. Afterwards, the lungs were placed in 30% sucrose for 6 h, then frozen in optimal cutting temperature (OCT) compound and placed into a cutting mold. The frozen blocks were sectioned at the UC San Diego Moores Cancer Center Histology Core. Each frozen slide was briefly fixed in 2% paraformaldehyde for 20 min then permeabilized with Triton-X100 for 5 min. A blocking solution containing 5% each donkey and goat serum was added to each slide for 1 h. Following blocking, the primary antibody solution containing 1% BSA and 0.1% Triton-X100 along with anti-CD68 (OriGene) and anti-GBS (Abcam) primary antibodies was added and incubated overnight. In other experiments, fluorescently-conjugated anti-CD68 (BioLegend) and anti-CD169/Sialoadhesin (BioLegend) antibodies were used in conjunction with the anti-GBS primary antibody (Abcam). The next day, each slide was washed thoroughly before the secondary antibody solution was added, containing anti-rat AlexaFluor-488 and anti-rabbit AlexaFluor-555, for 2 h. A DRAQ5 (ThermoFisher) solution was added for 25 min. Following staining, each slide was dried before a ProLong Gold anti-fade mountant (Life Technologies) was added dropwise. In some experiments, ProLong Gold anti-fade mountant with DAPI (Life Technologies) was added. Each slide was cured overnight. The next morning, each slide was sealed and imaged using a Leica TCS-SPE Confocal microscope at 100X, 400X and 630X magnification. For 4 color images, a Leica SP5 Confocal microscope at the UCSD Microscopy Core was used to image slides at 630X magnification.

Human lung macrophage gene expression
Human studies were reviewed and approved by the Institutional Review Board at the University of California, San Diego and Rady Children's Hospital. Tracheal aspirate macrophages were obtained via endotracheal suctioning as part of routine

respiratory care of intubated and mechanically ventilated patients born before 30 weeks gestation. Samples were obtained within the first 24 h of life and again on day 7. Macrophage RNA was isolated by TRIzol extraction and gene expression measured using Affymetrix GeneChip Human Transcriptome 2.0 Arrays.

Statistics
All statistical analyses were performed using GraphPad Prism 6. *P*-values < 0.05 were considered statistically significant and denoted with a single asterisk. *P*-values < 0.01 were denoted with two asterisks, *P*-values < 0.005 were denoted with three asterisks, and *P*-values < 0.001 were denoted with four asterisks. Experiments quantifying GBS bacteria and comparing cell surface expression were analyzed using the non-parametric Mann-Whitney U test. Experiments depicting the fold-change in mRNA expression were analyzed using the ΔC_T values between the gene of interest and the housekeeping gene GAPDH, and evaluated using the parametric unpaired t test.

Supplemental References

Chang, Y.-C., Olson, J., Beasley, F.C., Tung, C., Zhang, J., Crocker, P.R., Varki, A., and Nizet, V. (2014). Group B Streptococcus Engages an Inhibitory Siglec through Sialic Acid Mimicry to Blunt Innate Immune and Inflammatory Responses In Vivo. PLOS Pathogens *10*, e1003846.

Doran, K.S., Liu, G.Y., and Nizet, V. (2003). Group B streptococcal β-hemolysin/cytolysin activates neutrophil signaling pathways in brain endothelium and contributes to development of meningitis. The Journal of clinical investigation *112*, 736-744.

Hensler, M.E., Quach, D., Hsieh, C.-J., Doran, K.S., and Nizet, V. (2008). CAMP factor is not essential for systemic virulence of Group B Streptococcus. Microbial pathogenesis *44*, 84-88.

Lewis, A.L., Nizet, V., and Varki, A. (2004). Discovery and characterization of sialic acid O-acetylation in group B Streptococcus. Proc Natl Acad Sci U S A *101*, 11123-11128.

Wessels, M., Benedi, V., Kasper, D., Heggen, L., and Rubens, C. (1991). Type III capsule and virulence of group B streptococci. Genetics and molecular biology of streptococci, lactococci, and enterococci American Society for Microbiology, Washington, DC, 219-223.

Yim, H.H., Nittayarin, A., and Rubens, C.E. (1997). Analysis of the capsule synthesis locus, a virulence factor in group B streptococci. In Streptococci and the Host (Springer), pp. 995-997.